

Exclusive photosystem II photoinhibition derived from photoinactivation of oxygen-evolving complex in the marine angiosperm *Zostera marina*

Wei Zhao¹, Xiaoqi Yang², Ying Tan², Zhe Liu², Ming Yu Ma², Meng Xin Wang², Zimin Hu², and Quan sheng Zhang²

¹Affiliation not available

²Yantai University

July 16, 2020

Abstract

Photoinhibition is the popular topic in plant photosynthesis. However, restricted to experimental systems of *in vitro* membranes, knowledge of photosystem II (PSII) donor-side photoinhibition remains limited. Here, we report the first *in vivo* study of the mechanism in the marine higher plant *Zostera marina*. Preferential oxygen-evolving complex photoinactivation decreased the light-harvesting capacity and enhanced photosystem I cyclic electron flow (CEF). Non-photochemical quenching was inefficient and alternative electron flows, e.g. chlororespiration, Mehler reaction, malic acid synthesis, and photorespiration, remained unactivated, thereby reducing the unnecessary consumption of limited electron resources and maintaining a well carbon assimilation level. At variance with the PSII acceptor-side photoinhibition, the PSII photodamage of *Z. marina* was not attributed to ¹O₂ but was associated with the long-lived P680⁺ resulted from the photoinactivated OEC. Furthermore, we provided the novel insights into the PSII donor-side photoinhibition that rare PSII-CEF and ascorbate assumed photoprotective roles in *Z. marina*, which could donate electrons to the PSII reaction center to prevent the oxidative damage by P680⁺. This study addressed an important knowledge gap in PSII donor-side photoinhibition, providing a novel understanding of photosynthetic regulation mechanism responding to light stress.

Abstract

Photoinhibition is the popular topic in plant photosynthesis. However, restricted to experimental systems of *in vitro* membranes, knowledge of photosystem II (PSII) donor-side photoinhibition remains limited. Here, we report the first *in vivo* study of the mechanism in the marine higher plant *Zostera marina*. Preferential oxygen-evolving complex photoinactivation decreased the light-harvesting capacity and enhanced photosystem I cyclic electron flow (CEF). Non-photochemical quenching was inefficient and alternative electron flows, e.g. chlororespiration, Mehler reaction, malic acid synthesis, and photorespiration, remained unactivated, thereby reducing the unnecessary consumption of limited electron resources and maintaining a well carbon assimilation level. At variance with the PSII acceptor-side photoinhibition, the PSII photodamage of *Z. marina* was not attributed to ¹O₂ but was associated with the long-lived P680⁺ resulted from the photoinactivated OEC. Furthermore, we provided the novel insights into the PSII donor-side photoinhibition that rare PSII-CEF and ascorbate assumed photoprotective roles in *Z. marina*, which could donate electrons to the PSII reaction center to prevent the oxidative damage by P680⁺. This study addressed an important knowledge gap in PSII donor-side photoinhibition, providing a novel understanding of photosynthetic regulation mechanism responding to light stress.

Keywords: alternative electron donor; oxygen-evolving complex; P680⁺; PSII donor-side photoinhibition; *Zostera marina*

Introduction

Photosystem II (PSII) photoinhibition is commonly expected to occur when photosystems cannot sufficiently utilize the energy absorbed by their antenna system, its occurrence depends on the redox state of PSII acceptor components (Gururani et al., 2015). Strong illumination creates excessive excitation, which in turns leads to over-reduction of plastoquinone (PQ) acceptors, thus rendering the PSII reaction center (RC) inactive (Barber and Andersson, 1992; Melis, 1999). In contrast to acceptor-side photoinhibition, PSII donor-side photoinhibition is caused by water-splitting dysfunction, e.g., chemical damage like the removal of the Mn cluster by NH_2OH , Tris or high-salt washing (Callahan and Cheniae, 1985; Yadav and Pospíšil, 2012), and light damage like the photoinactivated oxygen-evolving complex (OEC) caused by direct UV illumination absorption (Yadav and Pospíšil, 2012; Havurinne and Tyystjärvi, 2017). These can be observed early in the photosynthetic membrane system *in vitro*. Recently, vulnerable OEC under visible wavelengths have also been reported *in vivo* in specific unicellular algae including the diatom *Phaeodactylum tricornutum* and the cyanobacteria *Synechocystis*, which are likely the result of a lack of photoprotective sunscreen compounds such as non-photosynthetic pigments or divinyl chlorophyll (Havurinne and Tyystjärvi, 2017; Soitamo et al., 2017). So far, *in vivo* PSII photoinhibition, derived from photoinactivated OEC, has not been demonstrated with direct experimental evidence in higher plants under visible light.

Several explicit characteristics of the mechanism can be summarized as follows: (1) the mechanism even occurs under low light conditions (Keren and Krieger-Liszkay, 2011); (2) non-photochemical quenching (NPQ) has low protective efficiency (Tyystjärvi, 2013); (3) the photoinhibition rate constant (K_{PI}) and light intensity are directly proportional (Tyystjärvi and Aro, 1996); (4) light leads to primary inactivation of OEC and secondary damage of PSII RC (Hakala et al., 2005; Tyystjärvi, 2008). The *in vitro* occurrence of donor-side photoinhibition, although mimicking, might not completely reflect *in vivo* phenomena (Dall'Osto et al., 2017) because of the incomplete photosynthetic apparatus. Restricted to imperfect experimental systems of photosynthetic membranes *in vitro*, knowledge of the mechanism remains limited and fragmented (Zavafer et al., 2015, 2017).

During PSII donor-side photoinhibition, the PSII RC may be susceptible to damage by both P680^+ and $^1\text{O}_2$ (Aro et al., 1993; Vass, 2011). When the electron donation of OEC is inferior to the rate of electron withdrawal by P680^{+*} (Vass, 2012), the long-lived P680^+ , a strong oxidant damaging component of PSII RC, is assumed to be a source of damage in this mechanism, which appears to be uncontroversial. However, whether the highly reactive $^1\text{O}_2$ is generated in the mechanism remains unclear, since the relevant results are mainly based on speculation and *in vitro* experiments (Nishiyama et al., 2011; Yadav and Pospíšil, 2012; Pospíšil, 2016). It has been considered that peroxidation of lipids by the highly oxidizing P680^+ and TyrZ^+ could cause $^1\text{O}_2$ formation (Yadav and Pospíšil, 2012; Pospíšil, 2016). The impaired OEC might damage specific oxygen channels that block oxygen molecules to P680 and conduct formative oxygen molecules outward, thus resulting in an accumulation of $^1\text{O}_2$ (Nishiyama et al., 2011). However, it has also been proposed that $^1\text{O}_2$ formation only occurs in preparations that contain functional OEC (Hideg et al., 1994; Johnson et al., 1995). When OEC is damaged, the redox potential of the $\text{Q}_\text{A}/\text{Q}_\text{A}^-$ pair shifts to a higher value, thus decelerating the conversion from $\text{P680}^+\text{Q}_\text{A}^-$ to $^3[\text{P680}^+\text{Phe}^-]$ (Ivanov et al., 2008). Even though the inactive OEC first promotes $^1\text{O}_2$ generation, conformational changes induced by the persistent OEC inactivity protects against $^1\text{O}_2$ formation (Tyystjärvi, 2008).

Ascorbate (AsA), as an alternative PSII electron donor, exerts a photoprotective role by continually supporting electron transport through PSII (Tóth et al., 2011). Although the amount of AsA and its affinity to PSII varies with species, this alternative electron transport appears to be ubiquitous in both plants and green alga, and serves a more vital protection in heat-stressed plants (Tóth et al., 2009). When the OEC in thylakoids is impaired, either by acidic pH or by UV-B exposure, AsA is also photooxidized at the donor side of PSII (Mano et al., 2004). During normal OEC function, no electrons are donated from AsA to PSII. It has thus been considered that the AsA acts as emergency electron donor when water oxidation is impaired (Mano et al., 2004). As another electron donation event, PSII cyclic electron flow (PSII-CEF), a pathway by which electrons on the Q_B site of PSII are returned to P680^+ via *cytb559*, has been reported to exert

a species-dependent role in photoprotection (Ananyev et al., 2017). Typically, strong light would lead to the over-reduction of Q_A through linear electron transfer, thereby enhancing the activity of PSII-CEF to consume the excess energy (Feikema et al., 2006; Lavaud, 2007). Other factors, such as nitrogen limitation which caused over-reduction of PQ pool, can stimulate the electron flow, thus preventing PSII RC photo-destruction (Wagner et al., 2016). PSII-CEF also plays a vital role in drought-tolerant species via proton gradient formation as a contribution to ATP production and photoprotection without consuming the limited water supply (Ananyev et al., 2016, 2017). Electron transport from PSII-CEF to PSII RC occurs when suppressed transfer of electrons from OEC to P680 extend the life time of $P680^+$ (Thompson and Brudvig, 1988; Miyake, 2002). Hence, it is reasonable to assume that both AsA and PSII-CEF can donate electrons to prevent the accumulation of the long-lived $P680^+$, exerting photoprotective roles during the PSII donor-side photoinhibition.

Zostera marina (Zosteraceae), a widespread seagrass species throughout the temperate northern hemisphere, playing ecological service function, evolved from a freshwater ancestor of terrestrial monocots and successfully adapted to a fully submerged marine environment (Wissler et al., 2011) where it must deal with shifted spectral composition, characterized by a high penetration of blue-green light (Olsen et al., 2016). The lack of cryptochrome blue-light receptors demonstrated by genome-based research in *Z. marina* (Olsen et al., 2016) would lead to insufficient anthocyanin levels (Li et al., 2013), thus weakening the screening of high-energy blue-green wavelengths (Hughes et al., 2010). Accordingly, *Z. marina* would possess more susceptible OEC with absorption peaks ranging between UV and blue-green light wavelengths (Tyystjärvi, 2008), providing the condition for the occurrence of PSII donor-side photoinhibition. Our recent study (Yang et al., 2017) showed that: (1) photoinhibition of *Z. marina* also occurred in low light conditions; (2) photoinhibition is closely relevant to the inactivation of OEC described by delayed fluorescence (DF); (3) the time-course changes of F_v/F_m exhibited the deficiency of the P_{fast} component of the Hanelt photoinhibition model, suggesting the slow NPQ development. These results agreed with the characteristics of PSII donor-side photoinhibition. Therefore, *Z. marina*, a marine angiosperm with complete photosynthetic apparatus and functional differentiation, may be a valid model species to study PSII donor-side photoinhibition.

In the present study, *in vivo* PSII photoinhibition derived from photoinactivated OEC under visible light was first determined in *Z. marina*, by identifying the primary target of the light-induced impairment. The integrated characteristics of the PSII photoinhibition associated with light absorption, electron transfer, and energy conversion were explored. Furthermore, damaging and photoprotective mechanisms were verified, based on the assumption that the alternative PSII electron donation pathways were activated to promote depletion of the long-lived $P680^+$.

Materials and methods

Sample preparation

Healthy *Z. marina* with intact rhizomes-systems was harvested on the sea floor at around 3 m depth near Rongcheng (37° 16'N, 122° 41'E) in the Weihai, Shandong province, China. Samples were precultured for 3 days in an aquarium under conditions of 15 °C and a 10: 14 light: dark cycle with a minimum saturation light intensity of 100 $\mu\text{mol photons m}^{-2}\text{s}^{-1}$. Prior to each experiment, each shoot was “standardized” to similar leaf morphology. Leaves for experimental measurement were collected from 2 cm above the sheath to keep the same age.

Experimental treatment

Prior to experimental treatment, pre-cultured *Z. marina* plants were dark-adapted overnight. To obtain the photoinhibition rate constant, *Z. marina* leaves were pre-incubated with lincomycin for 3 h in the dark and were then exposed to 20, 50, 100, 150, 200, 250, 300, 350, 400, 450, and 500 $\mu\text{mol photons m}^{-2}\text{s}^{-1}$ (μE) at 15 °C (Miyata et al., 2012). *Z. marina* leaves, which were dark-adapted and exposed to 300 μE for 3 h at 15 °C, were used for $^1\text{O}_2$ contents, AsA levels and chlorophyll a fluorescence measurement, and proteome analysis. The light intensity of 300 μE was approximated the maximum midday light intensity at the site of collection. The home-built LED lamps with color temperature of 6000 K and adjustable illumination intensity up to

1000 $\mu\text{mol photons m}^{-2} \text{ s}^{-1}$ were used for the sample preculture and light treatments. The spectrum of the home-built 6000 K LED lamp measured by HR-450 (HiPoint, China, Taiwan) has the main emission bands at around 450 nm (Fig. S2), similar with the spectrum of the 3 m depth under seawater where the plants are naturally located (Kirk, 2010; Olsen et al., 2016).

Due to lack of genetic operating system, the physiological roles of AsA and PSII-CEF were examined using inhibitors. PSII-CEF was inhibited or enhanced via incubation of 2,5-dimethyl-p-benzoquinone (DMBQ, TCI, Tokyo, Japan) at the concentration of 125 or 62 μM , respectively (Ananyev et al., 2016, 2017). AsA synthesis were inhibited via 50 μM rotenone purchased from Sigma-Aldrich (Millar et al., 2003; Garmier et al., 2008). Although the chloroplast NADPH dehydrogenase-like complex was also sensitive to rotenone (Garmier et al., 2008), no significant side effect of 50 μM rotenone was observed on PSI-CEF of *Z. marina* showed by the initial rate of P700⁺re-reduction ($V_{\text{re-red}}$, Fig. S3). To test the roles of AsA and PSII-CEF, four different combinations of AsA and PSII-CEF inhibitions were conducted: Light, Light + Rotenone, Light + DMBQ, and Light + Rotenone + DMBQ, forming the base of a factorial experimental design. Prior to exposure, *Z. marina* leaves saturated with filtered seawater or with the seawater solution containing inhibitors were incubated in the dark for 10 min at 15 °C. Moreover, leaves treated with 125 μM DMBQ or 50 μM rotenone under darkness for 190 min showed no significant changes in F_v/F_m (Fig. S4). A stock solution of 10 mM DMBQ and 25 mM rotenone was prepared with dimethyl sulfoxide whose concentration used in this study had no significant effect on *Z. marina* as indicated by F_v/F_m (Fig. S5).

Absorption spectrum and oxygen evolution measurements

To monitor the contents of AsA which could directly protect photosystems, AsA levels in chloroplasts were monitored by using vitamin C assay kit (A009, Nanjing Jiancheng Bioengineering Institute, Nanjing, China). ¹O₂ in chloroplasts contents were measured by using plant ROS singlet oxygen assay kit (GMS10150.4, GENMED, Boston, MA, USA). Chloroplasts were isolated from *Z. marina* leaves, which were dark-adapted and exposed to 300 μE for 3 h, by using the plants leaf chloroplast rude divide kit (GMS16004.1, GENMED). To monitor change in carbon fixation ability during 300 μE light exposure, the Rubisco carboxylase activity was determined by using ribulose biphosphate carboxylase/oxygenase (Rubisco) activity detection kit (BC0440, Solarbio, Beijing, China). Absorption measurements were performed using a multifunctional enzyme-labeled instrument (Tecan, Männedorf, Switzerland). O₂ evolution rate used to reflect the leaves photosynthetic rate was measured at 15 °C with a liquid-phase oxygen electrode system (Chlorolab2+, Hansatech, Norfolk, UK).

Chlorophyll a fluorescence and 820 nm modulated reflection (MR_{820nm}) measurements

A pulse-amplitude modulated fluorometer (Mini-PAM; Walz, Germany) was used to measure NPQ. During the course of measurements, the PAM fiber was placed in a fixed position at 60° in relation to *Z. marina* leaves to avoid shading or darkening.

Multi-function plant efficiency analyzer 2 (M-PEA-2; Hansatech, Hercules, UK) was used to simultaneously detect the kinetics of prompt fluorescence (PF), delayed fluorescence (DF), and MR_{820nm} and thus to monitor photochemical activity and dissect events in the electron transfer chain (Strasser et al., 2010; Gururani et al., 2015)^{10,62}. Changes in the OJIP fluorescence rise kinetics were assessed by calculating the difference value of variable fluorescence curves as $\Delta V_t = \Delta[(\Phi_t - \Phi_0) / (\Phi_{\infty} - \Phi_0)]$. Τη ρελατιε αριαβλε φλυορεσενζε ατ τηε Κ-στεπ (Ω_K) ωας αν ινδικατορ οφ τηε ΠΣΠ ελεςτρον δονατιον ζαπασιτψ (Στρασσερ, 1997· Βρεστις ετ αλ., 2012){Βρεστις, 2012 *265·Στρασσερ, 1997 *269}. Τηε δεσαψ κινετις οφ ΔΦ ατ μαξιμουμ I_1 ωερε φιττεδ ωιτη τηε φυνςτιον $\Delta\Phi(\tau) = L_1 \times \exp(-t/\tau_1) + L_2 \times \exp(-t/\tau_2) + L_3$, where L_1 and L_2 represent the amplitudes of the decay kinetics component and τ_1 and τ_2 represent their lifetimes (in ms), respectively. L_1 corresponded to the electron transport capacity at PSII donor side (Goltsev et al., 2009; Gao et al., 2013). MR_{820nm} obtained by a modulated measuring light at 820 nm was measured after far-red light was closed (Zhang et al., 2011). $V_{\text{re-red}}$, the initial rate of P700⁺re-reduction, was calculated to quantify PSI-CEF activity. Detailed calculations and physiological explanations of parameters are listed in Table S2.

Protein extraction, digestion, and tandem mass tag (TMT) labeling

TMT proteome of chloroplasts was adopted to identify differential proteins for achieving high-throughout and high-resolution screening. Chloroplasts were isolated from *Z. marina* leaves, which were dark-adapted (Dark) and exposed to 300 μE for 3 h (Light). The chloroplasts were suspended in BPP and Tris-saturated phenol, and then vortexed for 10 min. Proteins in the phenol phase collected via centrifugation at 12,000 g for 20 min were precipitated with ice-cold ammonium acetate, and then washed three times with 90% cooled acetone. The precipitate was dissolved in protein lysate (8 M urea, 1% SDS containing protease inhibitor), and the solution was then centrifuged as above to collect the protein supernatant. The above operations were performed at 4 °C. The protein concentration was measured by BCA.

Protein digestion was performed according to the standard procedure and the resulting peptide mixture was labeled using the 6-plex TMT reagents (ThermoFisher Scientific, Waltham, MA, USA). The peptides from Dark and Light samples were both labeled with TMT tags for three biological replicates. Briefly, each tube with 100 μg protein, containing 10 mM tris-(2-carboxyethyl)phosphine hydrochloride, was incubated at 37 °C for 60 min. The appropriate volume of iodoacetamide was added to a final concentration of 40 mM, and the solutions were incubated for 40 min in the dark. The samples were mixed with six volumes of cold acetone and the precipitates collected by centrifugation at 10,000 g for 20 min were resuspended with 100 μl 50 mM triethylammonium formate buffer. Trypsin solution was added to each sample tube according to a proportion of 1 : 50 (trypsin : protein) and the tubes were incubated overnight at 37 °C. The TMT reagent was added to corresponding peptide mixture respectively. All samples were then combined and vacuum dried.

High pH reversed-phase liquid chromatography separation

Samples were fractionated to increase the proteomic depth, using high pH reverse phase separation. The peptides resuspended in buffer A (2% acetonitrile, containing ammonium hydroxide solution, at pH 10) were separated by ACQUITY UPLC (Waters, Milford, MA, USA) connected to a high pH UPLC column. Gradient elution was achieved at a rate of 200 $\mu\text{l min}^{-1}$ for 66 min with buffer B (80% acetonitrile, containing ammonium hydroxide solution, at pH 10). Twenty fractions were collected from each sample and were pooled into 10 total fractions.

Liquid chromatography-mass spectrometry (LC-MS/MS) analysis

Mass spectrometry analysis was performed on a Q Exactive mass spectrometer coupled with Easy-nLC 1200 (ThermoFisher Scientific). The 2 μg peptides loaded onto the C18 column in buffer A (2% acetonitrile, 0.1% formic acid) were separated with a linear gradient of buffer B (80% acetonitrile and 0.1% formic acid) at a flow rate of 300 nl min^{-1} in Easy-nLC 1200. The eluted peptides were injected into a Q Exactive mass spectrometer (ThermoFisher Scientific), using 1.8 kV electrospray voltage. The acquisition of survey full-scan MS spectra (m/z 350-1300) was attributed to a mass resolution of 70,000, followed by 20 sequential high energy collisional dissociation MS/MS scans at a resolution of 35,000.

For protein identification, MS/MS spectra were searched using Protein DiscovererTM Software 2.2 and parent proteins were identified by the highest score for a given peptide mass. The following settings were used: a maximum of two miscleavages; carbamidomethylation of cysteines as fixed modification; protein N-terminal acetylation and oxidation of methionines as variable modifications. At least one unique peptide containing a minimum of six amino acids sequence was required for per protein. The false discovery rate (FDR) was set to 1% to validate peptide spectra.

Bioinformatics analysis

BLASTP was used to search homologous proteins for uncharacterized proteins defined by the *Z. marina* information category in Uniprot. Proteins with P -value < 0.05 and fold change (FC) > 1.2 were defined as DEPs. GO enrichment analysis of DEPs was performed using the Fisher's exact test and FDR correction. Protein-protein interaction (PPI) network was constructed using the STRING database with the Cytoscape software.

Western blotting

Western blotting was used to quantify OEC peripheral proteins PsbO, PsbP, PsbQ, as well as the terminal enzyme l-galactono-1,4-lactone dehydrogenase (GLDH) of AsA biosynthesis and PSII RC proteins D1, CP43. GLDH located in mitochondrion was detected using the proteins in leaves which were isolated as previously described (Jorriin-Novo, 2014). The other proteins located in photosynthetic membranes were detected using chloroplasts. To determine the loading quantity of sample, the protein and chlorophyll contents were measured as previously published (Porra et al., 1989). Solubilized materials were fractionated using sodium dodecyl sulfate–polyacrylamide gel electrophoresis. Western blot assays with antibodies (Agriser, Sweden) were performed as previously described (Fristedt et al., 2009). As equal loading control, the Rubisco large subunit (RbcL) antibody was used. The chemiluminescent bands visualized on a Gel Doc XR+ system (Bio-Rad, CA, USA) were quantified with the program Quantity One software. For each case, the density of the samples was standardized based on the RbcL density.

Statistical Analysis

Statistical analyses were performed using SPSS 22.0 statistical software package. All parameters were analyzed by one-way analysis of variance (ANOVA). Tukey’s tests were used to make post hoc comparisons. Repeated measures ANOVA was adopted to examine the effect of rotenone and DMBQ on F_v/F_m and W_k .

Data and materials availability

Raw MS and Proteome Discoverer output data have been uploaded to the iProX with ID: IPX0002022001. All other data needed to evaluate the conclusions in the paper are present in the paper and/or the Supplementary Materials. Additional data related to this paper may be requested from the authors.

Results

The category of PSII photoinhibition

The amplitude L_1 of the DF decay kinetics component declined significantly during the initial illumination already and continuously decreased with exposure duration (Fig. 1A), suggesting the decreased electron transport capacity of the PSII donor side following light exposure. As shown in Fig. 1B and C, the relative variable fluorescence at the K-step (W_K) was significantly increased and OEC peripheral proteins including the manganese-stabilizing protein PsbO and the Ca^{2+} -binding protein PsbP were significantly downregulated, confirming the partial impairment of OEC during the initial illumination. This decrease of OEC activity was accompanied by the decrease of PSII photochemical activity characterized by the decrease of F_p following light exposure (Fig. 1D). In the presence of lincomycin inhibiting D1 protein synthesis, the time-course changes in F_v/F_m under various photosynthetic photon flux density (PPFD) values fitted the first-order kinetics well (Fig. 1E). Both the decreased F_v/F_m even under ultra-dim light during the initial illumination and the direct proportionality of K_{PI} to PPFD from dim light to supersaturating light intensities further supported the occurrence of PSII donor-side photoinhibition in *Z. marina* (Fig. 1F).

Overview of quantitative proteome analysis

Among 2613 protein groups, a total of 2187 proteins were quantified with at least one unique peptide sequence (Fig. S1A). *Z. marina* samples were clustered and distinguished from each other based on light treatment (Fig. S1B). The 127 differentially expressed proteins (DEPs) were determined, which included 89 upregulated proteins and 38 downregulated proteins (Fig. S1C). Based on Gene ontology (GO) enrichment analysis, DEPs were classified into the following several biological processes: “photosystem II assembly”, “chlorophyll biosynthetic process”, “photosynthetic electron transport in photosystem I”, “regulation of photosynthesis, light reaction”, “PSII associated light-harvesting complex II catabolic process”, “response to light intensity”, and so on (Fig. 2A). In the Protein-protein interaction (PPI) network of the DEPs, OEC peripheral protein PsbO had a high degree of connectivity and strong interactions with other proteins (Fig. 2B), indicating that the photoinactivated OEC played a central role in the photosynthetic regulation of *Z. marina*.

Regulation of light capture

ATP-dependent zinc metalloprotease (FtsH) 4 and FtsH 2, both involved in “PSII associated light-harvesting complex II (LHCII) catabolic process”, were significantly upregulated (Fig. 2A). Three proteins responsible for antenna assembly, including LHCII protein Lhcb3, low PSII accumulation 3 (LPA3) assisting chlorophyll a binding protein CP43 assembly within PSII, and PsaH binding light-harvesting complex I protein Lhca2 to PSI core complex (Table S1), were downregulated, suggesting a decrease of antenna size following light exposure. The distinct interactions of PsbO with Lhcb3, PsaH were shown in the PPI network, indicating the potential of OEC to regulate antenna assembly (Fig. 2B).

Regulation of electron transport

Proteome data revealed that the proteins involved in PSII assembly, such as high chlorophyll fluorescence phenotype244 (HCF244), domain of unknown function (DUF1995) and thylakoid formation 1 (THF1), displayed upregulation expression, indicating that continuous repair was required to retain PSII functionality. The proteins involved in electron donating to PSI reaction center P700⁺, such as proton gradient regulation 5 (PGR5) and PsaN, were also upregulated, indicating the activation of the PGR5-dependent PSI-CEF (Fig. 2A). In addition, the protein called acclimation of photosynthesis to environment was upregulated, contributing to the acclimation of photosynthetic electron transfer to illumination (Table S1). The interactions between PsbO and HCF244, as well as PGR5 and PsaN, shown in the PPI network, suggested the need of electron transport regulation due to the partially impaired OEC (Fig. 2B).

Regulation of carbon fixation

Biological process enrichment analysis based on DEPs showed no significant change in the carbon fixation pathway at the protein level. However, both Glyceraldehyde-3-phosphate dehydrogenase (GAPDH) and phosphoribulokinase (PRK), involved in carbon fixation pathway, were dissociated from the GAPDH/CP12/PRK complex by the downregulated CP12, indicating the activation of GAPDH and PRK. Moreover, thioredoxin reductase (NTRC), which is associated with the activation of thioredoxins-regulated enzymes in carbon fixation pathway, was upregulated (Table S1). The good function of the carbon fixation pathway during photoinhibition was supported by the significantly increased carboxylase activity of ribulose biphosphate carboxylase/oxygenase (Rubisco) (Fig. 3A). Further supporting this function, photosynthetic rate characterized by O₂ evolution rate exhibited a typical photoinduction process followed by a normal level (Fig. 3A).

Energy dissipation

NPQ exhibited a decreasing tendency following a slow increase (Fig. 3B). The slow NPQ development followed a single exponential function and as a consequence fast-activated qE component was absent, while the NPQ_{max} showed a low value (Fig. 3C). Moreover, proteome data showed that the luminal pH sensor PsbS protein, which was required for qE, remained unchanged in response to light exposure (Table S1). Slightly upregulated zeaxanthin epoxidase (ZEP) and violaxanthin de-epoxidase (VDE) levels indicated a low level of xanthophyll cycle-dependent energy dissipation (Table S1). The two key enzymes of chlororespiration, post-illumination chlorophyll fluorescence increase and ubiquinol oxidase, remained unchanged. Similarly, D-glycerate 3-kinase, the core enzyme in photorespiration pathway, both ascorbate peroxidase (APX) and superoxide dismutase, the key enzymes of the Mehler reaction, and malate dehydrogenase, the key enzyme of malic acid synthesis, remained unchanged (Table S1). These results suggested that alternative electron flows associated with energy dissipation were not significantly activated.

Antioxidant system defense

Both the chlorophyll synthesis pathway and the early light-induced protein were not significantly induced by light exposure (Fig. 2A and Table S1), suggesting that there was no accumulation of free chlorophyll which would have acted as a generator of reactive oxygen species. Although Delta-aminolevulinic acid dehydratase, the enzyme committed to tetrapyrrole biosynthesis, and geranylgeranyl diphosphate reductase,

which provides phytol, were upregulated, the terminal key enzyme NADPH-protochlorophyllide oxidoreductase of chlorophyll synthesis was downregulated (Fig. 2A). The expression of the stromal antioxidant enzymes glutathione peroxidase (GPX) and APX remained unchanged (Table S1), further displaying that the antioxidant ability was not significantly enhanced following light exposure.

Damaging mechanism

Although the reduction of Q_A represented by $1 - V_J$ was significantly increased, the reduction degree of Q_A was low (by $\sim 4.5\%$) (Fig. 4A). Consistently, no significant increases in chloroplast 1O_2 content and, the quencher of 1O_2 , GPX were observed following light exposure (Fig. 4A and Table S1), while PsbH, which stabilized the combination of PSII and β -carotene associated with scavenging 1O_2 , was significantly downregulated (Table S1). Nevertheless, PSII photochemical activity significantly decreased, indicated by a decrease in F_P and an increase in F_O following light exposure (Fig. 4B). This suggested the existence of an additional source of damage other than 1O_2 .

Photoprotective mechanisms

l-galactono-1,4-lactone dehydrogenase (GLDH), the terminal enzyme in the major Smirnov-Wheeler pathway for AsA biosynthesis, together with the AsA level in the chloroplast were significantly upregulated after light exposure (Fig. 5A), providing a clue to AsA being the alternative electron donor. Additionally, analysis of the K step in ΔV_t curves and F_P in OJIP curves showed: there was the lower PSII electron donation capacity and PSII photochemical activity induced by 125 μ M DMBQ binding at the PQ site to uncouple PSII-CEF, compared to 62 μ M DMBQ binding at the Q_B site to enhance PSII-CEF (Fig. 5B). This suggested that PSII-CEF serves as a possible alternative electron donation pathway.

To test the roles of AsA and PSII-CEF in safeguarding PSII function, a factorial design experiment with different combinations of rotenone and DMBQ, the inhibitors of AsA and PSII-CEF, was conducted. Compared with F_v/F_m values, the order of PSII activity was: Light > Light + Rotenone > Light + DMBQ > Light + Rotenone + DMBQ (Fig. 6A). Simultaneously, inhibition of AsA synthesis or uncoupling of PSII-CEF led to the further decreased PSII electron donation capacity indicated by W_K , and the decrease was more obvious during the late illumination (Fig. 6A). Furthermore, Western-blotting analyses showed no visible changes of D1, CP43 proteins after light exposure and their degradation was detected after both inhibitor treatments, indicating that AsA and PSII-CEF prevented the damage of PSII RC via donating electrons (Fig. 6B). The suppression of temporary electron donor and the alternative electron flow also led to a further impairment of OEC, as characterized by the distinct degradation of PsbO and PsbP proteins (Fig. 6B).

Discussion

The evidence presented here, at both spectral and protein levels, confirmed that OEC of *Z. marina* was preferentially inactivated in response to light exposure: (1) PSII electron donation capacity characterized by L_1 and W_K was significantly decreased already during initial illumination; (2) OEC activity represented by the contents of OEC peripheral proteins (Bricker and Frankel, 2008; Popelkova et al., 2011) greatly decreased, while the reduction degree of Q_A at the acceptor-side, represented by $1 - V_J$, slightly increased; (3) PSII photoinhibition occurred upon light exposure and the photoinhibition rate constant, determined via first-order kinetic fits, was positively correlated with PPFD at all tested light intensities. This was the first *in vivo* study of PSII donor-side photoinhibition with the direct experimental evidence in higher plants under visible light. The *in vivo* occurrence of this mechanism in higher plants enabled the study of both integrated photosynthetic characteristics and photoprotective mechanisms, which involved multiple coordinated systems.

The present study investigated the integrated photosynthetic regulatory mechanisms involved in light absorption, transfer and conversion, and energy dissipation via chloroplast proteome combined with chlorophyll fluorescence phenotype. The strong interactions of PsbO with Lhcb3, PGR5, HCF244, Psb29, PsaN, and PsaH, shown in the PPI network, suggested that OEC played a central role in the regulation of photosynthe-

sis. The decreased size of the PSI and PSII antennas indicated a decline of the light-harvesting capacity in *Z. marina*. The interactions of PsbO with PsaH and Lhcb3 were interpreted as a need to decrease the light-harvesting capacity due to the partially impaired OEC. It should be realized that a decrease of PSII antenna size corresponds to fewer absorbed photons but also to a faster trapping rate (Croce and Van Amerongen, 2014). Simultaneously, PSII assembly was activated to retain PSII functionality. Because continuously impaired OEC led to a relatively oxidized PQ pool (Makarova et al., 2007), the PGR5-dependent PSI-CEF in *Z. marina* was activated to supplement the PSI linear electron transport. Activated PSI-CEF revealed by proteome data in the present study was in agreement with chlorophyll fluorescence physiological phenotype observed in our previous study (Yang et al., 2017). The interactions between PsbO and HCF244, as well as PGR5 and PsaN indicated the potential of the partially impaired OEC to enhance PSII repair and activate the PGR5-dependent PSI-CEF.

Continuous impairment of OEC in this mechanism suggested electron deficiency in the electron transport chain. Unchanged antioxidant levels and unactivated alternative electron flows, such as chlororespiration, Mehler reaction, malic acid synthesis and photorespiration, supported this viewpoint. The low PSII excitation pressure caused by electron deficiency made it difficult to form a strong trans-thylakoid proton gradient (ΔpH), and consequently, could not induce strong NPQ. This was verified by the unchanged ΔpH sensor PsbS protein, the low value of NPQ_{max} (Schubert et al., 2015), and slightly upregulated ZEP and VDE. NPQ is usually dissected into at least three kinetic components, in which qE, induced within 20-60 s, was the dominant NPQ component (Horton et al., 1996; Nilkens et al., 2010). Further examination of the dynamics of NPQ induction in *Z. marina* indicated the absence of the fast qE component, which accounted for the slow development of NPQ. Moreover, the decrease of NPQ during the late illumination indicated that the demand for dissipation decreased with the increased OEC impairment. A low NPQ capacity has also been reported in the seagrass *Posidonia sinuosa* (Schubert et al., 2015).

The low levels of NPQ were conducive to the formation of the reduced form of NADPH and ATP derived from photosynthetic electron transport, which in turn contributed to carbon fixation. In C3 plants, photosynthesis is typically restricted by the Rubisco capacity due to its exceedingly low catalytic turnover rate and competition with oxygenation reaction (Farquhar et al., 1980). The significantly enhanced carboxylase activity of Rubisco and the upregulated NTRC (Nikkanen et al., 2016) suggested an increased CO_2 fixation rate in response to light exposure. Recoveries of activities of GAPDH and PRK, the key enzymes of carbon fixation, were achieved by downregulated CP12 (Marri et al., 2009), suggesting the activation of carbon fixation pathway. The well photosynthetic performance during photoinhibition was also supported by the normal photosynthetic rate characterized by O_2 evolution rate in *Z. marina*.

$^1\text{O}_2$ is usually formed by a photosensitization reaction in which an oxygen molecule reacts with $^3\text{P680}$ (Pospíšil, 2016). The sensitizer molecule $^3\text{P680}$, produced by $^3[\text{P680}^+\text{Phe}^-]$ which is generated either via spin conversion of primary radical pair $\text{P680}^+\text{Phe}^-$ or via recombination of $\text{P680}^+\text{Q}_\text{A}^-$, is triggered by the over-reduction of Q_A (Vass et al., 1992; Hakala et al., 2005; Ohnishi et al., 2005; Vass, 2011). The reduction degree of Q_A was low in *Z. marina*, which was evidenced by a slight decrease of $1 - V_j$. Therefore, the conditions for $^1\text{O}_2$ production were not appropriate. In fact, light exposure neither caused an upregulation of PsbH and GPX, nor an increase of $^1\text{O}_2$ levels. The strong interaction between PsbO and PsbH indicated that there was no need for PsbH to stabilize the combination of excess β -carotene and PSII (Hall et al., 2016) to eliminate $^1\text{O}_2$. Moreover, the inhibition of alternative electron donation in our study resulted in a significant damage of PSII RC described by the net losses of D1 and CP43 proteins, indicating that the photodamage of PSII was attributed to the long-lived P680^+ rather than $^1\text{O}_2$. Thus, the long-lived P680^+ resulted from the interrupted electron supply was usually considered as the damage source in the PSII donor-side photoinhibition, which has been suggested by Vass (2012) and Tyystjärvi (2008). Noticeably, a distinct low descending amplitude of F_v/F_m was observed during light exposure, which could be explained by most PSII RC remaining open to contribute to the depletion of the pool of high-potential P680^+ via facilitating the direct charge recombination of the $\text{P680}^+\text{Q}_\text{A}^-$. Because the competition between $^3[\text{P680}^+\text{Phe}^-]$ formation and the direct recombination of the $\text{P680}^+\text{Q}_\text{A}^-$ was controlled by PSII excitation pressure (Vass and Cser, 2009), the low reduction degree of Q_A in *Z. marina* prevented the formation of $^3[\text{P680}^+\text{Phe}^-]$.

The existence of alternative PSII electron donors has been reported in some species (Thompson and Brudvig, 1988; Toth et al., 2009, 2011). Based on *in vivo* data, the increased AsA level and the upregulated GLDH content involved in AsA synthesis following light exposure provided a clue of AsA as alternative electron donor. Similarly, in contrast to 62 μM DMBQ enhancing PSII-CEF, 125 μM DMBQ uncoupling PSII-CEF induced the lower PSII electron donation capacity and PSII photochemical activity, providing a clue of PSII-CEF as another alternative donation pathway. Furthermore, a factorial design experiment with different combinations of AsA and PSII-CEF inhibitions demonstrated that the suppression of alternative electron donation damaged the PSII component, including a decrease in F_v/F_m , an increase in W_K , as well as net losses of PSII RC proteins and OEC peripheral proteins. With the duration of light exposure, the inhibition effect became more significant, of which, the most severe damage of PSII was caused by the dual inhibition of AsA and PSII-CEF. Based on these results, we suggested that both AsA and PSII-CEF were important photoprotective mechanisms, which provided electrons to remit the oxidative stress from long-lived P680^+ during light exposure.

In conclusion, the water-splitting dysfunction caused by OEC photoinactivation interrupted the electron supply from water to the oxidized primary donor P680^+ , resulting in the damage to the PSII RC of *Z. marina*. At least PSII-CEF and the alternative donor AsA exerted photoprotective roles in the depletion of P680^+ by donating electrons to PSII (Fig. 7). In contrast to acceptor-side photoinhibition caused by electron excess, continuous impairment of OEC resulted in electron deficiency in the electron transport chain during the PSII photoinhibition. For the efficient use of the limited electrons, NPQ was inefficient and the alternative electron flows associated with energy dissipation, such as chlororespiration, Mehler reaction, malic acid synthesis and photorespiration, were not significantly activated to decrease unnecessary consumption (Fig. 7). The extremely sensitivity of OEC to visible light was presumably a result of insufficient polyphenol levels caused by a lack of blue light photoreceptors in a habitat that is rich in blue light (Peng and Moriguchi, 2013; Jiang et al., 2016).

Acknowledgments

This work was financially supported by the National Natural Science Foundation of China (No. 41376154). We wish to thank E. Tyystjärvi (University of Turku) for constructive suggestions to the improvement of this manuscript.

References

- Ananyev G., Gates C. & Dismukes G. C. (2016). The O_2 quantum yield in diverse algae and cyanobacteria is controlled by partitioning of flux between linear and cyclic electron flow within photosystem II. *Biochimica et Biophysica Acta (BBA) - Bioenergetics*, 1857, 1380-1391.
- Ananyev G., Gates C., Kaplan A. & Dismukes G. C. (2017). Photosystem II-cyclic electron flow powers exceptional photoprotection and record growth in the microalga *Chlorella ohadii*. *Biochimica et Biophysica Acta (BBA) - Bioenergetics*, 1858, 873-883.
- Aro E. M., Virgin I. & Andersson B. (1993). Photoinhibition of Photosystem II. Inactivation, protein damage and turnover. *Biochimica et Biophysica Acta (BBA) - Bioenergetics*, 1143, 113-134.
- Barber J. & Andersson B. (1992). Too much of a good thing: light can be bad for photosynthesis. *Trends in Biochemical Sciences*, 17, 61-66.
- Brestic M., Zivcak M., Kalaji H. M., Carpentier R. & Allakhverdiev S. I. (2012). Photosystem II thermostability *in situ*: Environmentally induced acclimation and genotype-specific reactions in *Triticum aestivum* L. *Plant Physiology & Biochemistry*, 57.
- Bricker T. M. & Frankel L. K. (2008). The *psbO1* Mutant of *Arabidopsis* Cannot Efficiently Use Calcium in Support of Oxygen Evolution by Photosystem II. *Journal of Biological Chemistry*, 283, 29022-29027.
- Callahan F. E. & Cheniae G. M. (1985). Studies on the photoactivation of the water-oxidizing enzyme : I. Processes limiting photoactivation in hydroxylamine-extracted leaf segments. *Plant Physiology*, 79, 777-786.

- Croce R. & Van Amerongen H. (2014). Natural strategies for photosynthetic light harvesting. *Nature Chemical Biology*, 10, 492.
- Dall'osto L., Cazzaniga S., Bressan M., Paleček D., Židek K., Niyogi K. K., Fleming G. R., Zigmantas D. & Bassi R. (2017). Two mechanisms for dissipation of excess light in monomeric and trimeric light-harvesting complexes. *Nature Plants*, 3, 17033.
- Eberhard S. & Finazzi Gwollman F. A. (2008). The dynamics of photosynthesis. *Annual Review of Genetics*, 42, 463-515.
- Farquhar G. D., Von Caemmerer S. V. & Berry J. A. (1980). A biochemical model of photosynthetic CO₂ assimilation in leaves of C₃ species. *Planta*, 149, 78-90.
- Feikema W. O., Marosvölgyi M. A., Lavaud J. & Gorkom H. J. V. (2006). Cyclic electron transfer in photosystem II in the marine diatom *Phaeodactylum tricornutum*. *BBA - Bioenergetics*, 1757, 829-834.
- Fristedt R., Willig A., Granath P., Crèvecoeur M., Rochaix J.-D. & Vener A. V. (2009). Phosphorylation of photosystem II controls functional macroscopic folding of photosynthetic membranes in *Arabidopsis*. *The Plant Cell*, 21, 3950-3964.
- Gao J., Li P., Ma F. & Goltsev V. (2013). Photosynthetic performance during leaf expansion in *Malus micromalus* probed by chlorophyll a fluorescence and modulated 820 nm reflection. *J Photochem Photobiol B*, 137.
- Garmier M., Carroll A. J., Delannoy E., Vallet C., Day D. A., Small I. D. & Millar A. H. (2008). Complex I dysfunction redirects cellular and mitochondrial metabolism in *Arabidopsis*. *Plant Physiology*, 148, 1324-1341.
- Goltsev V., Zaharieva I., Chernev P. & Strasser R. J. (2009). Delayed fluorescence in photosynthesis. *Photosynthesis Research*, 101, 217.
- Gururani M. A., Venkatesh J. & Tran L. S. P. (2015). Regulation of photosynthesis during abiotic stress-induced photoinhibition. *Molecular Plant*, 8, 1304-1320.
- Hakala M., Tuominen I., Keränen M., Tyystjärvi T. & Tyystjärvi E. (2005). Evidence for the role of the oxygen-evolving manganese complex in photoinhibition of Photosystem II. *Biochimica et Biophysica Acta (BBA) - Bioenergetics*, 1706, 68-80.
- Hall J., Renger T., Müh F., Picorel R. & Krausz E. (2016). The lowest-energy chlorophyll of photosystem II is adjacent to the peripheral antenna: Emitting states of CP47 assigned via circularly polarized luminescence. *Biochimica Et Biophysica Acta*, 1857, 1580-1593.
- Havurinne V. & Tyystjärvi E. (2017). Action spectrum of photoinhibition in the diatom *Phaeodactylum tricornutum*. *Plant & Cell Physiology*, 58, 2217-2225.
- Hideg , Spetea C. & Vass I. (1994). Singlet oxygen and free radical production during acceptor- and donor-side-induced photoinhibition. Studies with spin trapping EPR spectroscopy. *Biochimica et Biophysica Acta (BBA) - Bioenergetics*, 1186, 143-152.
- Horton P., Ruban A. & Walters R. (1996). Regulation of light harvesting in green plants. *Annual Review of Plant Physiology and Plant Molecular Biology*, 47, 655-684.
- Hughes N. M., Morley C. B. & Smith W. K. (2010). Coordination of anthocyanin decline and photosynthetic maturation in juvenile leaves of three deciduous tree species. *New Phytologist*, 175, 675-685.
- Ivanov A. G., Sane P. V., Hurry V., quist G. & Huner N. P. A. (2008). Photosystem II reaction centre quenching: mechanisms and physiological role. *Photosynthesis Research*, 98, 565-574.
- Jiang M., Ren L., Lian H., Liu Y. & Chen H. (2016). Novel insight into the mechanism underlying light-controlled anthocyanin accumulation in eggplant (*Solanum melongena* L.). *Plant Science*, 249, 46-58.

- Johnson G. N., Rutherford A. W. & Krieger A. (1995). A change in the midpoint potential of the quinone QA in Photosystem II associated with photoactivation of oxygen evolution. *Biochimica et Biophysica Acta (BBA) - Bioenergetics*, 1229, 202-207.
- Jorin-Novo J. V. (2014). Plant proteomics methods and protocols. *Methods in Molecular Biology*, 1072, 3-13.
- Keren N. & Krieger-Liszkay A. (2011). Photoinhibition: molecular mechanisms and physiological significance. *Physiologia Plantarum*, 142, 1-5.
- Kirk J. T. O. (2010). The nature of the underwater light field.
- Lavaud J. (2007). Fast regulation of photosynthesis in diatoms: mechanisms, evolution and ecophysiology. *Functional Plant Science and Biotechnology*, 1, 267-287.
- Li L., Aro E. M. & Millar A. H. (2018). Mechanisms of photodamage and protein turnover in photoinhibition. *Trends in Plant Science*, 23, 667-676.
- Li Y. Y., Mao K., Zhao C., Zhao X. Y., Zhang R. F., Zhang H. L., Shu H. R. & Hao Y. J. (2013). Molecular cloning and functional analysis of a blue light receptor gene MdCRY2 from apple (*Malus domestica*). *Plant Cell Reports*, 32, 555-566.
- Makarova V. V., Kosourov S., Krendeleva T. E., Semin B. K., Kukarskikh G. P., Rubin A. B., Sayre R. T., Ghirardi M. L. & Seibert M. (2007). Photoproduction of hydrogen by sulfur-deprived *C. reinhardtii* mutants with impaired photosystem II photochemical activity. *Photosynthesis Research*, 94, 79-89.
- Mano J. I., Eva H. & Asada K. (2004). Ascorbate in thylakoid lumen functions as an alternative electron donor to photosystem II and photosystem I. *Archives of Biochemistry & Biophysics*, 429, 71-80.
- Marri L., Zaffagnini M., Collin V., Issakidis-Bourguet E., Lemaire S. D., Pupillo P., Sparla F., Miginiac-Maslow M. & Trost P. (2009). Prompt and easy activation by specific thioredoxins of Calvin cycle enzymes of *Arabidopsis thaliana* associated in the GAPDH/CP12/PRK supramolecular complex. *Molecular Plant*, 2, 259-269.
- Melis A. (1999). Photosystem-II damage and repair cycle in chloroplasts: what modulates the rate of photodamage in vivo? *Trends in Plant Science*, 4, 130-135.
- Millar A. H., Mittova V., Kiddle G., Heazlewood J. L., Bartoli C. G. & Theodoulou (2003). Control of ascorbate synthesis by respiration and its implications for stress responses. *Plant Physiology*, 133, 443-447.
- Miyake C., Yonekura, K., Kobayashi, Y., & Yokota, A (2002). Cyclic electron flow within PSII functions in intact chloroplasts from spinach leaves. *Plant and Cell Physiology*, 43, 951-957.
- Miyata K., Noguchi K. & Terashima I. (2012). Cost and benefit of the repair of photodamaged photosystem II in spinach leaves: roles of acclimation to growth light. *Photosynthesis Research*, 113, 165-180.
- Nikkanen L., Toivola J. & Rintamäki E. (2016). Crosstalk between chloroplast thioredoxin systems in regulation of photosynthesis. *Plant Cell & Environment*, 39, 1691-1705.
- Nilkens M., Kress E., Lambrev P., Miloslavina Y., Müller M., Holzwarth A. R. & Jahns P. (2010). Identification of a slowly inducible zeaxanthin-dependent component of non-photochemical quenching of chlorophyll fluorescence generated under steady-state conditions in *Arabidopsis*. *Biochimica et Biophysica Acta (BBA) - Bioenergetics*, 1797, 466-475.
- Nishiyama Y., Allakhverdiev S. I. & Murata N. (2011). Protein synthesis is the primary target of reactive oxygen species in the photoinhibition of photosystem II. *Physiologia Plantarum*, 142, 35-46.
- Ohnishi N., Allakhverdiev S. I., Takahashi S., Higashi S., Watanabe M., Nishiyama Y. & Murata N. (2005). Two-step mechanism of photodamage to photosystem II: step 1 occurs at the oxygen-evolving complex and step 2 occurs at the photochemical reaction center. *Biochemistry*, 44, 8494-9.

- Olsen J. L., Rouzé P., Verhelst B., Lin Y. C., Bayer T., Collen J., Dattolo E., De P. E., Dittami S. & Maumus F. (2016). The genome of the seagrass *Zostera marina* reveals angiosperm adaptation to the sea. *Nature*, 530, 331-335.
- Peng T. & Moriguchi T. (2013). The molecular network regulating the coloration in apple. *Scientia Horticulturae*, 163, 1-9.
- Popelkova H., Boswell N. & Yocum C. (2011). Probing the topography of the photosystem II oxygen evolving complex: PsbO is required for efficient calcium protection of the manganese cluster against dark-inhibition by an artificial reductant. *Photosynthesis Research*, 110, p.111-121.
- Porra R., Thompson W. & Kriedemann P. (1989). Determination of accurate extinction coefficients and simultaneous equations for assaying chlorophylls a and b extracted with four different solvents: verification of the concentration of chlorophyll standards by atomic absorption spectroscopy. *Biochimica et Biophysica Acta (BBA) - Bioenergetics*, 975, 384-394.
- Pospíšil P. (2016). Production of reactive oxygen species by photosystem II as a response to light and temperature stress. *Frontiers in Plant Science*, 7, 1950.
- Schubert N., Ia M., Colombo-Pallota F. & Iquez S. E. (2015). Leaf and canopy scale characterization of the photoprotective response to high-light stress of the seagrass *Thalassia testudinum*: High-light response in a seagrass. *Limnology & Oceanography*, 60, 286-302.
- Soitamo A., Havurinne V. & Tyystjärvi E. (2017). Photoinhibition in marine picocyanobacteria. *Physiologia Plantarum*, 161, 97-108.
- Strasser B. J. (1997). Donor side capacity of Photosystem II probed by chlorophyll a fluorescence transients. *Photosynthesis Research*, 52, 147-155.
- Strasser R. J., Tsimilli-Michael M., Qiang S. & Goltsev V. (2010). Simultaneous in vivo recording of prompt and delayed fluorescence and 820-nm reflection changes during drying and after rehydration of the resurrection plant *Haberlea rhodopensis*. *Biochimica et Biophysica Acta (BBA) - Bioenergetics*, 1797, 1313-1326.
- Tóth S. Z., Nagy V., Puthur J. T., Kovács L. & Garab G. (2011). The physiological role of ascorbate as photosystem II electron donor: protection against photoinactivation in heat-stressed leaves. *Plant Physiology*, 156, 382-392.
- Tóth S. Z., Puthur J. T., Nagy V. & Garab G. (2009). Experimental evidence for ascorbate-dependent electron transport in leaves with inactive oxygen-evolving complexes. *Plant Physiology*, 149, 1568-1578.
- Thompson L. K. & Brudvig G. W. (1988). Cytochrome b-559 may function to protect photosystem II from photoinhibition. *Biochemistry*, 27, 6653-6658.
- Tyystjärvi E. (2008). Photoinhibition of Photosystem II and photodamage of the oxygen evolving manganese cluster. *Coordination Chemistry Reviews*, 252, 361-376.
- Tyystjärvi E. (2013). Photoinhibition of photosystem II. *Int Rev Cell Mol Biol*, 300, 243-303.
- Tyystjärvi E. & Aro E. M. (1996). The rate constant of photoinhibition, measured in lincomycin-treated leaves, is directly proportional to light intensity. *Proceedings of the National Academy of Sciences of the United States of America*, 93, 2213-2218.
- Vass I. (2011). Role of charge recombination processes in photodamage and photoprotection of the photosystem II complex. *Physiologia Plantarum*, 142, 6-16.
- Vass I. (2012). Molecular mechanisms of photodamage in the Photosystem II complex. *Biochimica et Biophysica Acta (BBA) - Bioenergetics*, 1817, 209-217.
- Vass I. & Cser K. (2009). Janus-faced charge recombinations in photosystem II photoinhibition. *Trends in Plant Science*, 14, 200-205.

Vass I., Styring S., Hundal T., Koivuniemi A., Aro E. M. & Andersson B. (1992). Reversible and irreversible intermediates during photoinhibition of photosystem II: stable reduced QA species promote chlorophyll triplet formation. *Proceedings of the National Academy of Sciences of the United States of America*, 89, 1408-1412.

Wagner H., Jakob T., Lavaud J. & Wilhelm C. (2016). Photosystem II cycle activity and alternative electron transport in the diatom *Phaeodactylum tricornutum* under dynamic light conditions and nitrogen limitation. *Photosynthesis Research*, 128, 151-161.

Wissler L., Codoñer F. M., Gu J., Reusch T. B., Olsen J. L., Procaccini G. & Bornberg-Bauer E. (2011). Back to the sea twice: identifying candidate plant genes for molecular evolution to marine life. *BMC Evolutionary Biology*, 11, 8.

Yadav D. K. & Pospíšil P. (2012). Evidence on the formation of singlet oxygen in the donor side photoinhibition of photosystem II: EPR spin-trapping study. *Plos One*, 7, e45883.

Yang X. Q., Zhang Q. S., Zhang D. & Sheng Z. T. (2017). Light intensity dependent photosynthetic electron transport in eelgrass (*Zostera marina* L.). *Plant Physiology & Biochemistry*, 113, 168-176.

Zavafer A., Cheah M. H., Hillier W., Chow W. S. & Takahashi S. (2015). Photodamage to the oxygen evolving complex of photosystem II by visible light. *Scientific Reports*, 5, 16363.

Zavafer A., Koinuma W., Chow W. S., Cheah M. H. & Mino H. (2017). Mechanism of photodamage of the oxygen evolving Mn cluster of photosystem II by excessive light energy. *Scientific Reports*, 7, 1-8.

Zhang Z., Jia Y., Gao H., Zhang L., Li H. & Meng Q. (2011). Characterization of PSI recovery after chilling-induced photoinhibition in cucumber (*Cucumis sativus* L.) leaves. *Planta*, 234, 883-889.

Figure Legends

Fig. 1 Preferential impairment of OEC induced by light. (A) Variations in the amplitude L_1 of the kinetics component calculated by fitting the DF decay kinetics to the time function $DF(t) = L_1 \times \exp(-t/\tau_1) + L_2 \times \exp(-t/\tau_2) + L_3$. The inset shows DF decay kinetics at I_1 in response to light exposure. (B) Changes in the relative variable fluorescence at the K-step (W_k) in response to light exposure. (C) Variations in OEC peripheral proteins PsbO, PsbP and PsbQ during light exposure. Values were % of dark 100% and normalized to RbcL amount. The significantly different value (Tukey's tests, $P < 0.05$) from 0 min or dark is marked with an asterisk (*). (D) Changes in the normalized chlorophyll fluorescence intensity of OJIP transients (F_t/F_o) in response to light exposure and plotted on a logarithmic time scale. (E and F) Photoinhibition measured by the decrease in F_v/F_m in the presence of lincomycin. (E) The decreases of F_v/F_m standardized based on 0 min fitted well with the function $F_v/F_m = \exp(-K_{PI} \times t)$ (all R^2 values > 0.9). (F) Dependence of the K_{PI} on photon flux density ($P < 0.05$). The means \pm s.d. were calculated from three independent samples. The means \pm s.d. were calculated from three independent samples. Each curve represents the average of three replicates.

Fig. 2 GO enrichment analysis and PPI network of DEPs. (A) The biological processes in GO enrichment analysis of DEPs. The DEPs are on the left and the GO pathway names are on the right ($P < 0.05$). (B) PPI network of DEPs. Red nodes indicate upregulated proteins and blue nodes indicate downregulated proteins. The larger size of the node represented the higher connectivity of the protein, which indicated more interactions with other proteins. The width of the line represents the capacity of the interaction between proteins.

Fig. 3 Photosynthetic activity and NPQ response to light exposure. (A) Changes in O_2 evolution rate and Rubisco carboxylase activity in response to light exposure. The significantly different value (Tukey's tests, $P < 0.05$) from 0 min is marked with an asterisk (*). (B) chlorophyll fluorescence during NPQ formation. (C) The kinetics of NPQ induction fitted with the function $NPQ = A \times \exp(-x/t) + y_0$. The means \pm s.d. were calculated from three independent samples.

Fig. 4 The relevant parameters of PSII damage response to light exposure. (A) Variations in probabilities for an electron moving further than $Q_A(1-V_J)$ and chloroplast¹O₂ contents after light exposure. The significantly different value from Dark (Tukey's tests, $P < 0.05$) is marked with an asterisk (*). (B) Changes in OJIP transients in response to light exposure and plotted on a logarithmic time scale. The means \pm s.d. were calculated from three independent samples. Each curve represents the average of three replicates.

Fig. 5 AsA and PSII-CEF response to light exposure.(A) Variations in GLDH contents determined by densitometry and chloroplast AsA levels in response to light exposure. The significantly different value from 0 min (Tukey's tests, $P < 0.05$) is marked with an asterisk (*). (B) Changes in chlorophyll a fluorescence kinetics as summarized by ΔV_t and OJIP curves in response to light exposure and different concentrations of DMBQ. The signals are plotted on a logarithmic time scale. Each curve represents the average of three replicates.

Fig. 6 Photoprotection of AsA and PSII-CEF response to light exposure. (A) Time course of the changes in maximal photochemical yield of the PSII (F_v/F_m) and the relative variable fluorescence at the K-step (W_K) in response to different inhibitors. The significant effects of rotenone and DMBQ on F_v/F_m and W_K during HL exposure were examined with repeated measures ANOVA (all p values < 0.05). (B) The changes in PSII RC proteins D1, CP43 and OEC peripheral proteins PsbO, PsbP, PsbQ after 3 h of treatment. Values were % of dark 100% and normalized to RbcL amount. The significantly different value from 0 min (Tukey's tests, $P < 0.05$) is marked with an asterisk (*). Data are expressed as mean \pm s.d. ($n = 3$).

Fig. 7 Schematic model of donor-side photoinhibition derived from the photoinactivated OEC. The red arrows represent the activated pathways in which the degree of activation are represented by the width of line and the dark arrows represent the pathways that were not significantly activated. Positions of photosynthetic complexes in thylakoid membrane are based on published annotations (Eberhard and Finazzi GWollman, 2008; Gururani et al., 2015; Li et al., 2018). PQ, plastoquinone; Cytb6f, cytochrome b6f; PC, plastocyanin; Fd, ferredoxin; FNR, ferredoxin NADP⁺ reductase; MDA, monodehydroascorbate; Mal, malate; PTOX, ubiquinol oxidase; GLYK, D-glycerate 3-kinase; MDH, malate dehydrogenase; OAA, oxaloacetic acid; SOD, superoxide dismutase; APX, ascorbate peroxidase.

Supporting Information

Fig. S1 Overview of the identified proteins. (a) Protein profile statistical information. (b) The principal component analysis (PCA) of identified proteins. (c) Volcano plots of proteins with differential expression in Light vs. Dark group. Blue nodes indicate significantly downregulated proteins ($n = 38$); red nodes represent upregulated proteins ($n = 89$).

Fig. S2 Normalized spectral power distribution of the 6000 K LED lamp used in the experiments.

Fig. S3 The effect of 50 μ M rotenone on the initial rate of P700+ re-reduction (Vre-red) following light exposure of 3 h. There was no significant difference between Light and Light + Rotenone treatments (Tukey's tests, $P > 0.05$). Data are expressed as mean \pm s.d. ($n = 3$).

Fig. S4 The effect of 50 μ M rotenone and 125 μ M DMBQ on F_v/F_m under darkness for 190 min. There was no significant difference of F_v/F_m between the three treatments (Tukey's tests, all p values > 0.05). Data are expressed as mean \pm s.d. ($n = 3$).

Fig. S5 The effect of 1.45% (v/v) dimethyl sulfoxide (DMSO) on OJIP transients and F_v/F_m following light exposure of 3 h. There was no significant difference of F_v/F_m between Light and Light + DMSO treatments (Tukey's tests, $P > 0.05$). Data are expressed as mean \pm s.d. ($n = 3$).

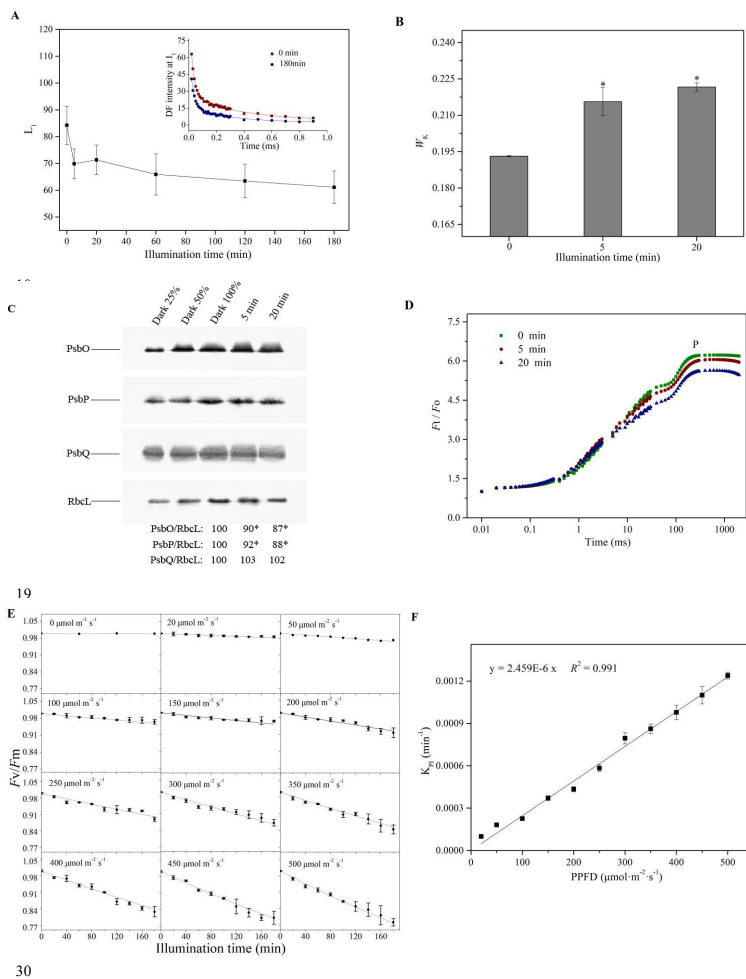
Table S1 List of 32 proteins identified by TMT in *Z. marina* following light exposure.

Table S2 Chlorophyll fluorescence parameters used in the study.

Hosted file

Figures.pdf available at <https://authorea.com/users/342396/articles/469220-exclusive-photosystem-ii-photoinhibition-derived-from-photoinactivation-of-oxygen-evolving-complex-in-the-marine-angiosperm-zostera-marina>

1 Figures



30